

Stage of Charge Estimation of a Lithium-ion Battery Based on the Interactive Multi-model

Yongqin Zhou¹, Qiujiu Zhu^{1,*}, Yongchao Wang¹, Ce Huang², Ran Li¹, Yujia Chang³

¹ School of Electrical and Electronic Engineering, Harbin University of Science and Technology, Harbin 150080, China

² School of measurement and communication engineering, Harbin University of Science and Technology, Harbin 150080, China

³ State Grid Harbin Electric Power Supply Company, Harbin 150000, China

*E-mail: 2652673847@qq.com

Received: 15 February 2022 / Accepted: 7 April 2022 / Published: 7 May 2022

In order to address issues affecting the estimation accuracy of the state of charge (SOC) in the state of health (SOH) of lithium-ion batteries throughout their whole life cycle, this paper proposed a method to estimate the SOC of lithium-ion batteries based on the Interacting Multiple Model (IMM). By establishing multiple battery models with different degrees of aging in the parallel filtering process of IMM, the likelihood function was used to calculate the model probability of a single model. Moreover, the state estimates of multiple single models were then fused and output, solving the poor SOC estimation accuracy due to battery aging. The method was subsequently verified on multiple sets of randomly aging battery data via experimentation, for which the findings indicated that the proposed method was able to accurately track battery SOC and perform real-time estimation of battery capacity.

Keywords: Lithium-ion battery; SOC; SOH; IMM

1. INTRODUCTION

As a carrier for the storage and transformation of electrical energy, lithium-ion batteries can be converted into energy with extremely high efficiency without pollutant emissions, which are currently being widely applied in electric vehicles [1,2]. Accurate estimation of the state of lithium-ion batteries serves as the basis for ensuring the normal operation of lithium-ion batteries. However, as the number of battery cycles increases, the degree of aging also increases, and the internal parameters undergo nonlinear changes, which leads to the difficulty of SOC estimation in Battery Life Cycle. Therefore, developing a method that is able to accurately estimate the SOC during the entire life cycle of a lithium-ion battery is necessary.

Currently, numerous methods for studying the SOC estimation of lithium-ion batteries exist, which can be generally divided into open-loop-based methods, data-driven methods, and model-based methods [3].

Open loop methods include ampere-hour integration and open circuit voltage [4-7]. Specifically, ampere-hour integration is simple to apply and encompasses few calculations. Moreover, it can guarantee accuracy when used within a short period of time. However, in this method, the initial value of the SOC must be calibrated, where errors can accumulate. The number of errors is relatively large under high temperature conditions and severe current fluctuations. Therefore, when used alone, the estimation accuracy of this method may not be guaranteed [8]. Meanwhile, the open circuit voltage method involves measuring the open circuit voltage of the battery, which then calculates the remaining power of the battery through the relationship of OCV-SOC. The calculation is simple to compute, however, the open circuit voltage of the battery needs to be measured offline, which is not suitable for an actual battery management system [9].

The data-driven method is equivalent to a black box model and does not require factoring in the relationship between various parameters or an accurate battery model – it only requires a large amount of data for learning to complete battery SOC estimation [10,11]. Guo et al.[12] employed a GA-BP neural network to train battery data to estimate SOC. Liu et al.[13] combined a BP neural network algorithm with a genetic algorithm, which was able to estimate the SOC value of the battery in real-time, thereby improving the estimation accuracy of the SOC. In addition, Zhang et al.[14] proposed a sparse learning machine method based on the traditional least square support vector machine (LS-SVM) formula for the estimation of SOC. Venkatesan et al.[15] adopted six machine learning algorithms (ANN, SVM, LR, GPR, EBa and EBo) to estimate the SOC of lithium-ion battery systems in electric vehicles, where ANN and GPR were found to be best. However, the above algorithm was took into account a large amount of experimental data, had a long computational time and required enough storage space in order to attain success. Batteries may not meet the above requirements in actuality, thus restricting data-driven methods' wide application in battery SOC estimation [16].

Model-based methods include the electrochemical model and equivalent circuit model. The electrochemical model constructs the model by studying the chemical reaction mechanism of the battery, which is too complicated and confers high computational costs; thus, it is difficult to be applied practically [17,18]. The equivalent circuit model involves constructing basic circuit devices so as to simulate the resistance and capacitance characteristics of the battery. Here, the parameters of the device in the model have actual physical meanings, reflecting the chemical reactions at different stages within the battery. Through the device parameters in the model, the SOC and load, as well as the relationship between voltage and load current, can establish the equation of state, which finally estimates the SOC of the battery through a filter. This method is simple and practical and has clear physical meaning, high accuracy, low complexity, and low cost, which has been widely applied [19].

Xia et al.[20] used electrochemical impedance spectroscopy in order to demonstrate that as the health and aging level of lithium-ion batteries increases, the series resistance value in the equivalent circuit model increases, capacitance value of the CPE (Constant Phase Element) component decreases, and model parameters undergo large changes. Chen et al.[21] verified the linear relationship between the ohmic internal resistance of the battery and capacity attenuation, in which a battery SOH estimation

method was proposed that was based on the relationship between ohmic internal resistance and capacity attenuation. Xiong et al.[22] put forward that the battery model parameter set possesses time-varying characteristics, that is, when the battery ages, the equivalent circuit model parameters change in a wide range. Xia et al.[23] proposed that the zero-crossing frequency of the battery impedance phase can reflect the aging state of the battery. Specifically, as the battery ages, its impedance will change significantly. The above studies pointed out that as the battery ages, the battery model parameters will change greatly. Fang et al.[24] established a second-order equivalent circuit model of a lithium-ion battery, adopted the forgetting factor recursive least square algorithm (FFRLS) in completing online parameter identification, and used the double extended Kalman filter algorithm (DEKF) to achieve the SOC of estimates. Westerhoff et al.[25] estimated the SOC by establishing the relationship between each component and SOC in an equivalent circuit model of a lithium-ion battery. Guo et al.[26] and Huang et al.[27] used the second-order equivalent circuit as the battery model, and used the extended Kalman filter (EKF) algorithm and improved extended Kalman filter algorithm to estimate the SOC, respectively. Wang et al.[28] established a second-order equivalent model of lithium-ion batteries and proposed a method for estimating the SOC of lithium-ion batteries based on a weighted adaptive recursive least square method and extended Kalman filter. Zhao et al.[29] established the second-order equivalent circuit model of the battery through the HPPC method, and then estimated the SOC of the battery through the strong tracking Kalman filter algorithm. The above studies, however, did not consider the impact of battery aging on equivalent circuit parameters when estimating the SOC. When the battery ages, the parameters of the equivalent circuit model will change greatly, resulting in a decrease in the robustness of the SOC estimation method and affecting the estimated accuracy of the SOC. In order to address battery aging's impact on the accuracy of SOC estimation, Lee et al.[30] used a multilayer neural network model in order to model the SOH neural network, using a multilayer neural network or long and short-term memory to estimate the SOC. Although the SOC of the battery can be accurately estimated under different aging states, a large amount of training data is required. Moreover, the algorithm is complicated, has high calculation costs, and is not suitable for practical applications. Kim et al.[31] established an adaptive hybrid battery model that combines the enhanced SOC estimation Coulomb counting algorithm as well as the equivalent circuit model. Here, the variable-length sliding window least squares (VSWLS) online parameter identification algorithm was used to estimate the battery model. In terms of electrical parameters, an adaptive discrete-time sliding-mode observer (ADSMO) was used to estimate the battery SOC and SOH, however, it is complicated to model and has low accuracy. Li et al.[32] used a dual adaptive extended Kalman filter to estimate the SOC and SOH of the battery. Although the influence of aging on the accuracy of SOC estimation was considered, a single model was adopted, the estimation accuracy of SOC was low, the algorithm was complicated, and the amount of calculation was large, which is not suitable for practical applications. Xia et al.[33] and Xia et al.[34] used the interactive multi-model-based extended Kalman filter algorithm and the interactive multi-model-based Cubature Kalman filter algorithm to estimate the SOC of the battery, respectively. The experimental results show that, compared with the traditional extended Kalman filter algorithm and Cubature Kalman filter algorithm, the algorithm based on interactive multi-model has higher estimation accuracy in estimating SOC.

In order to address issues of SOC estimation in the whole life cycle of lithium-ion batteries, this paper proposes an SOC estimation algorithm based on the Interacting Multiple Model (IMM) [35]. First,

through the FFRLS algorithm, multiple equivalent circuit models of the lithium-ion battery under different aging states are obtained to form a battery multi-model simulation system. Each equivalent circuit model is described by a strong tracking Kalman filter (STKF), in which all Kalman filters work independently and in parallel. The state of the lithium-ion battery is then estimated according to the input information, and the probability of each equivalent circuit model is calculated. Through the weighted fusion of information, the estimated values of SOC and SOH in the current state of the battery can be calculated while simultaneously calculating the estimated values of the state variables of the battery simulation system at the current time. The model probability as well as the estimated value of the state variable at the current moment are subsequently fed back to the input terminal, and the input information is then interactively updated by the Markov chain. As the battery runs cyclically, the proposed IMM algorithm is shown to accurately estimate the SOC value throughout the battery's full life cycle. The innovations of the proposed algorithm for the life cycle SOC estimation of lithium-ion batteries are:

1) In IMM, the Markov transition probability matrix controls the conversion and information interaction between the aging models. The difference between the measured and estimated values of each aging model is the residual, and the probability of the current battery matching each model can be then calculated based on the residual. The probability is called the model probability, and then the state estimation value and corresponding model probability are weighted and fused to output to remedy the decline in SOC estimation accuracy due to battery aging.

2) IMM integrates the output of each filter in order to estimate battery SOC and accurately estimates the maximum usable capacity of the battery, which is able to perform accurate tracking of the battery SOC as well as real-time estimation of battery capacity.

3) Compared with EKF and UKF, STKF produces smaller approximation errors when dealing with nonlinear systems, improves the robustness of the model, and has a strong ability to track slow and sudden changes, which makes it very suitable for combination with IMM as the filtering algorithm for battery SOC estimation.

The overall structure of the article is organized as follows:

The second-order RC equivalent circuit model is established in Section 2, after which the method of parameter identification used in the model is introduced. The third section specifically elaborates the SOC estimation algorithm of IMM in the battery life cycle. The fourth section outlines experiments that verified the advantages of the proposed algorithm in the SOC estimation accuracy and estimation speed during the battery life cycle. The fifth section summarizes the main conclusions of this article.

2. BATTERY EQUIVALENT CIRCUIT MODEL AND PARAMETER IDENTIFICATION

2.1 Establishment of an equivalent circuit model

Investigating the external characteristics of the battery during operation by modeling the battery, which also serves as the basis in estimating battery SOC and SOH. Battery models can be divided into equivalent circuit models, data-driven models and electrochemical models [36,37]. Numerous considerations are taken into account in electrochemical modeling. The complexity of the model is high, which is difficult to realize in engineering. Generally, it is only used as a means of battery performance

analysis. In terms of data-driven modeling, a large amount of experimental data is required, the number of calculations is large, and the network parameter selection and accuracy of training samples are extremely dependent. In addition, the training method has a significant influence on the error. The equivalent circuit model is able to systematically reflect the working characteristics of the battery with low complexity, low difficulty, easy calculation, and feasible application in engineering. Currently, commonly used equivalent circuit models of lithium-ion batteries include the Rint model, Thevenin model, PNGV model, Randles model and RC model [38]. The Rint model is the simplest equivalent circuit model, which is composed of an ohmic internal resistance R_0 and constant voltage source U_{oc} in series. It is difficult to accurately describe the nonlinear output characteristics of lithium-ion batteries with low accuracy [39]. The Thevenin model is based on the Rint model and has a RC loop connected in series that is used to simulate the polarization of the battery; however, the accuracy of the first-order RC circuit is poor, hence, the second-order equivalent circuit model is usually used [40]. Shrivastava et al.[41] introduced a second-order RC model composed of two sets of RCs as well as a resistor in series, which also considered the influence of concentration polarization. Accordingly, the simulation accuracy was found to be higher, while the characteristics were shown to be closer to those of a real battery. Newman et al.[42] put forward that calculating the second-order equivalent circuit model is moderate, the model accuracy is high, and it is closer to the real battery characteristics. Considering the accuracy and computational complexity of the battery model, this paper adopted the second-order RC equivalent circuit model as the battery model, which is depicted below.

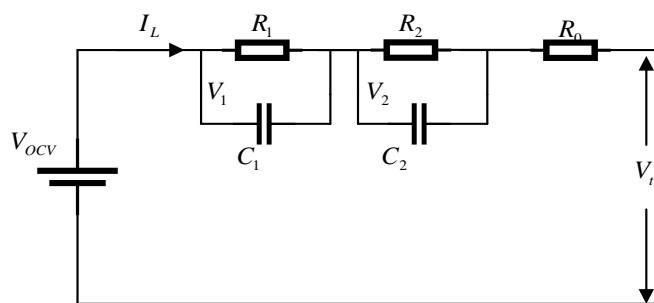


Figure 1. Second Order RC equivalent circuit diagram.

As shown in Fig. 1, R_0 stands for the internal ohmic resistance of the battery, V_{ocv} is the open-circuit voltage of the battery, C_1, C_2 are the capacitor which are representation of the polarization effects, R_1, R_2 are the resistance which are representation of the polarization effects, V_t is the battery terminal voltage, and I_L is the charging current or discharging current.

According to the second-order RC equivalent circuit model of the battery, the terminal voltage of the battery is:

$$V_t = I_L R_0 + V_1 + V_2 + V_{ocv} \tag{1}$$

I_L is negative when the battery is discharging and positive when charging. The voltages across capacitors C_1 and C_2 are:

$$\dot{V}_1 = -\frac{V_1}{R_1 C_1} + \frac{I_L}{C_1} \tag{2}$$

$$\dot{V}_2 = -\frac{V_2}{R_2 C_2} + \frac{I_L}{C_2} \tag{3}$$

SOC calculation formula is:

$$SOC = SOC(0) - \frac{\eta}{Q_r} \int_0^{\tau} I_L(t) dt \tag{4}$$

SOC(0) is the initial state of SOC, then η is the Coulombic efficiency and Q_r is the rated capacity of the battery.

The open circuit voltage V_{OCV} of the battery is basically equal to the electromotive force of the battery, and it has a functional relationship with the battery SOC, It could be expressed as:

$$V_{OCV} = f(SOC) \tag{5}$$

In this paper, a constant current discharge method is used to perform the 10th-order data with SOC, and the equation is as follows:

$$V_{ocv} = a_0 + a_1 SOC^{10} + a_2 SOC^9 + a_3 SOC^8 + a_4 SOC^7 + a_5 SOC^6 + a_6 SOC^5 + a_7 SOC^4 + a_8 SOC^3 + a_9 SOC^2 + a_{10} SOC \tag{6}$$

The V_{OCV} -SOC curve is fitted according to the above formula (6), as shown in Fig. 2. As battery operating conditions change, there are some changes about the trend of the OCV-SOC of the battery. Accordingly, the coefficients in equation (6) need to be updated to further modify the parameters of the equivalent circuit.

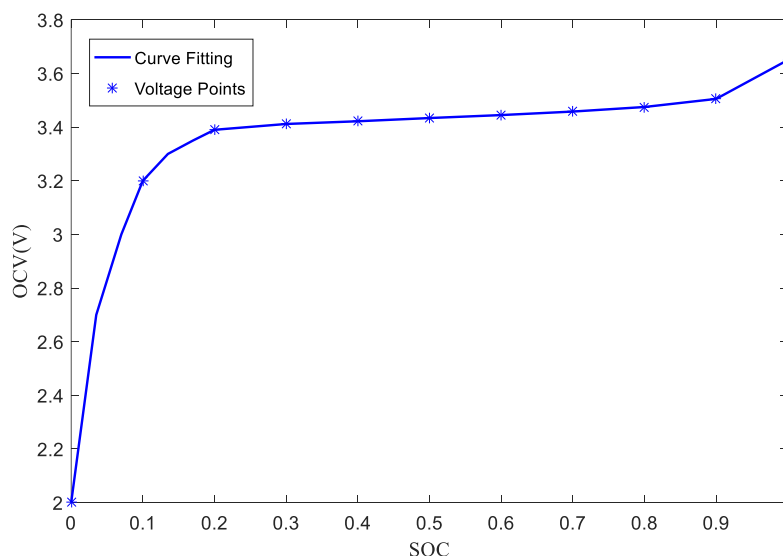


Figure 2. V_{OCV} -SOC fitting curve.

Discretize (1), (2), (3) and (4) to obtain the battery state equation and measurement equation as follows:

$$\begin{bmatrix} SOC_k \\ V_{1,k} \\ V_{2,k} \end{bmatrix} = \begin{bmatrix} 1 & 0 & 0 \\ 0 & e^{-T/\tau_1} & 0 \\ 0 & 0 & e^{-T/\tau_2} \end{bmatrix} \times \begin{bmatrix} SOC_{k-1} \\ V_{1,k-1} \\ V_{2,k-2} \end{bmatrix} + \begin{bmatrix} -\eta T / Q_r \\ R_1(1-e^{-T/\tau_1}) \\ R_2(1-e^{-T/\tau_2}) \end{bmatrix} \times I_{L,k} + \begin{bmatrix} w_{1,k} \\ w_{2,k} \\ w_{3,k} \end{bmatrix} \quad (7)$$

$$Z_k = \begin{bmatrix} \frac{V_{ocv,k} - I_{L,k}R}{SOC_k} & -1 & -1 \end{bmatrix} \times \begin{bmatrix} SOC_k \\ V_{1,k} \\ V_{2,k} \end{bmatrix} + v_k \quad (8)$$

where, $V_{OCV,k} = f(SOC_k)$.

The control variable is $I_{L,k}$, the observation variable is Z_k , and the state variable is $X_k = [SOC_k \ V_{1,k} \ V_{2,k}]$.

The system state equation and measurement equation of the battery model are:

$$\begin{cases} X_k^j = f_{k-1}^j(X_{k-1}^j, \Phi_{k-1}) + w_{k-1}^j = A_{k-1}^j X_{k-1}^j + B_{k-1}^j \Phi_{k-1} + w_{k-1}^j \\ Z_k = h_k^j(X_k^j, \Phi_k) + v_k = C_k^j X_k^j + v_k \end{cases} \quad (9)$$

where X_{k-1}^j is the state variable of the system, Φ_k is the control variable of the system, f and h are nonlinear functions, Z_k represents the observation variable of the system, v_k and w_k^j are the measurement noise and process noise of the system, respectively, both of which conform to Gaussian distribution. Additionally, the variance is R_k and Q_k , respectively.

By comparing (7), (8) and (9), each coefficient can be determined:

$$A_{k-1}^j = \begin{bmatrix} 1 & 0 & 0 \\ 0 & e^{-T/\tau_1^j} & 0 \\ 0 & 0 & e^{-T/\tau_2^j} \end{bmatrix}, \quad B_{k-1}^j = \begin{bmatrix} -\eta T / Q_r \\ R_1^j(1-e^{-T/\tau_1^j}) \\ R_2^j(1-e^{-T/\tau_2^j}) \end{bmatrix}, \quad C_k = \begin{bmatrix} \frac{V_{ocv,k} - I_{L,k}R}{SOC_k} & -1 & -1 \end{bmatrix}$$

2.2 Parameter identification

Parameter identification methods of the lithium-ion battery equivalent circuit model are divided into offline identification and online identification [43]. Lithium-ion batteries have very obvious nonlinear characteristics during the charge and discharge processes. Moreover, parameters in the second-order equivalent circuit model vary with the number of cycles, charge and discharge current, temperature, SOC and SOH, which adopt fixed model parameters. Accordingly, in order to estimate the SOC of the battery, the errors will continue to increase [44]. Therefore, the offline method cannot be used to identify the parameters of the model. In order to be able to track and correct the model parameters in real time, this paper adopted the Recursive Least Squares Method based on the forgetting factor to identify the model parameters online [45]. The recursive least squares algorithm does not require storage of all monitoring data; rather, it can be estimated online. Adding the forgetting factor may result in the reduction of the influence of old data on the result, which is relatively stable in correcting parameter estimation and encompasses a small amount of calculation, thus improving the identification result with better accuracy and in real-time [46-48]. Therefore, this paper used FFRLS to identify the battery model parameter R_0, R_1, R_2, C_1, C_2 .

$$\hat{\theta}(K+1) = \hat{\theta}(k) + K(k+1)[y(k+1) - \phi^T(k+1)\hat{\theta}(k)] \quad (10)$$

$$K(k+1) = P(k)\phi(K+1)[\lambda + \phi^T(k+1)P(k)\phi(K+1)]^{-1} \quad (11)$$

$$P(k+1) = \frac{1}{\lambda}[I - K(k+1)\phi^T(k+1)]P(k) \quad (12)$$

In the above formulae, $K(k)$ represents the gain matrix, $y(k)$ represents the output k -th observation matrix, $P(k)$ represents the covariance matrix of the k -th calculation, $\phi(k)$ represents the observation vector, I represents the identity matrix, and $\theta(k)$ represents the parameter matrix that needs to be identified in the model. λ is the forgetting factor, for which its value range is generally $[0.95, 1]$ [49], which is $\lambda = 0.984$ in the paper.

According to the second-order RC equivalent circuit shown in Fig. 1, the input of the battery multi-model simulation system was the terminal current $I_{L,k}$; the output $V_{t,k}$ was the difference between the open-circuit voltage $V_{OCV}(k)$ and the load voltage $V_m(k)$ (where $m = 1, 2$). $V_{OCV}(k)$ was gained from equation (6) above.

According to Laplace transform and Kirchhoff's voltage law, the formula for the complex frequency domain of the battery open circuit voltage was:

$$V_{OCV} = I_L(k)(R_0 + \frac{R_1}{1 + R_1C_1S} + \frac{R_2}{1 + R_2C_2S}) + V_m(k) \quad (13)$$

Where, $\tau_1 = R_1C_1$, $\tau_2 = R_2C_2$; τ_1 , τ_2 were the polarization time constant and concentration time constant respectively.

According to (13):

$$\begin{aligned} \tau_1\tau_2V_{OCV}s^2 + V_{OCV}s(\tau_1 + \tau_2) + V_{OCV} &= \tau_1\tau_2R_0I_L(k) + \\ [R_1\tau_2 + R_2\tau_1 + R_0(\tau_1 + \tau_2)]I_L(k)s + (R_0 + R_1 + R_2)I_L(k) & \quad (14) \\ + \tau_1\tau_2V_m(k)s^2 + (\tau_1 + \tau_2)V_m(k)s + V_m(k) & \end{aligned}$$

Let:

$$\begin{cases} a = R_0 = \tau_1\tau_2 \\ b = \tau_1 + \tau_2 \\ c = R_0 + R_1 + R_2 \\ d = R_1\tau_2 + R_2\tau_1 + R_0(\tau_1 + \tau_2) \end{cases} \quad (15)$$

Substituting (15) into (14) :

$$\begin{aligned} aV_{OCV}s^2 + bs(\tau_1 + \tau_2) + V_{OCV} &= aR_0s^2 + dI_L(k)s + \\ cI_L(k) + aV_m(k)s^2 + bV_m(k)s + V_m(k) & \quad (16) \end{aligned}$$

Let:

$$\begin{cases} s = \frac{x(k) - x(k-1)}{T^2} \\ s^2 = \frac{x(k) - 2x(k-1) + x(k-2)}{T^2} \end{cases} \quad (17)$$

where T represented the sampling period, $T = 1$ second.

Combine the above formulas (16) and (17) :

$$\begin{aligned}
 V_{OCV}(k) - V_m(k) &= \frac{-b - 2a}{1 + a + b} [V_{OCV}(k - 1) - V_m(k - 1)] + \\
 &\frac{a}{1 + a + b} [V_{OCV}(k - 2) - V_m(k - 2)] + \frac{aR_0 + c + d}{1 + a + b} I_L(k) + \\
 &\frac{-2a_0 - d}{1 + a + b} I_L(k - 1) \times \frac{aR_0}{1 + a + b} I_L(k - 2)
 \end{aligned} \tag{18}$$

The elements in $\theta(k)$ were:

$$\left\{ \begin{aligned}
 k_1 &= \frac{-2a - b}{1 + a + b} \\
 k_2 &= \frac{a}{1 + a + b} \\
 k_3 &= \frac{aR_0 + c + d}{1 + a + b} \\
 k_4 &= \frac{-2a_0 - d}{1 + a + b} \\
 k_5 &= \frac{aR_0}{1 + a + b}
 \end{aligned} \right. \tag{19}$$

By sorting out (19):

$$\left\{ \begin{aligned}
 R_1 &= \frac{\tau_1 c + \tau_2 R_0 - d}{\tau_1 - \tau_2} \\
 R_2 &= c - R_0 - R_1 \\
 C_1 &= \frac{\tau_1}{R_1} \\
 C_2 &= \frac{\tau_2}{R_2}
 \end{aligned} \right. \tag{20}$$

The parameters of the battery second-order equivalent circuit model can be expressed by the following formula (21):

$$V_m(k) = \phi^T(k) \hat{\theta} + \xi(k) \tag{21}$$

where, $\theta = [k_1 \ k_2 \ k_3 \ k_4 \ k_5]$, $\phi^T(k) = [V_m(k - 1) \ V_m(k - 2) \ I_L(k) \ I_L(k - 1)]$.

According to the above formulas (19)-(21), various parameters of the battery model can be obtained.

In order to verify the performance of the FFRLS identification circuit model parameters proposed in this paper, experiments were performed under BB DST (Beijing bus dynamic stress test) conditions for verification purposes. First, the current in working conditions was used as the excitation, and the estimated value of the terminal voltage output by the model and actual value of the terminal voltage output by the battery were then selected as the comparison value. Fig. 3 shows the results of the parameter identification, and the experiment lasted for 3000s. According to Fig.3, at the beginning and end of the experiment, the error of the terminal voltage was noted to be large, the change in the middle process was relatively stable, and the error was small. The maximum error reached 38.5mV, which was

only 1.2% of the rated voltage. During the whole experiment, the root mean square error and average absolute error of the terminal voltage were 21.9mV and 20.5mV, respectively.

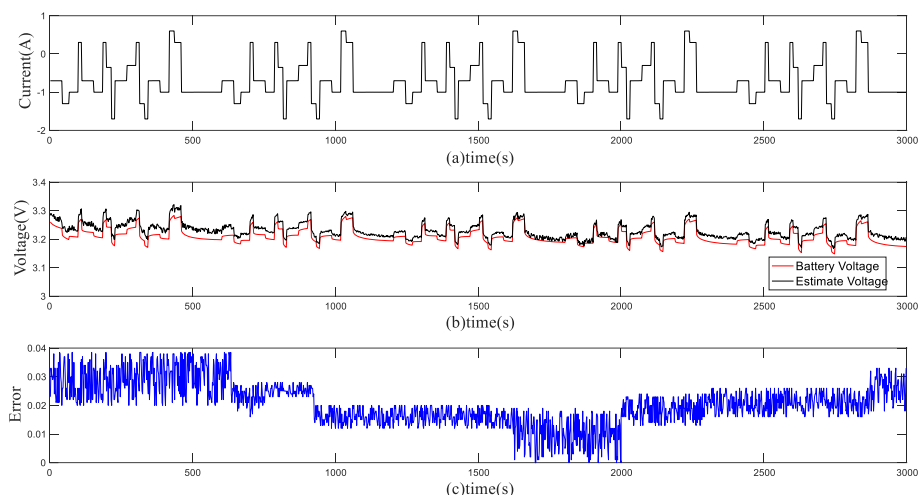


Figure 3. BBDST experiment: (a) BBDST current curve; (b) comparison curve between model output terminal voltage and battery output terminal voltage; (c) error curve of voltage at both ends.

The BBDST experiment demonstrated that FFRLS was able to accurately predict the model parameters, and the error was small, which did not appear to increase over time. Therefore, parameter identification based on FFRLS has better robustness and can make the battery run stably in different working environments. By identifying the parameters of the battery model under different aging states, the second-order equivalent circuit model of the battery under the corresponding state can be obtained.

3. SOC ESTIMATION ALGORITHM BASED ON INTERACTIVE MULTIPLE MODELS

The interactive multi-model estimation theory uses a set of filters that are independent and work in parallel. Each filter represents a different aging model of the battery that estimates battery state from system inputs and measured variables in order to obtain the estimated SOC and SOH output by the model. They are then weighted and fused with the estimated state value as well as the corresponding model probability so as to obtain an accurate estimation of battery SOC and SOH. The information interactions and conversion between the equivalent circuit models are determined by a Markov transition probability matrix (TPM) [50]. The difference between the actual and estimated values of the aging model is the residual, and the probability of the current battery matching the model is calculated based on the residual. This probability is called the model probability [51,52].

Fig. 4 below represents the flow chart of the interactive multi-model (IMM) algorithm. IMM assumed that the battery has j battery aging models to form a set $\{ STKF1, STKF2, STKF3, \dots, STKFj \}$. Each filter represented an aging model, and each aging model is able to estimate the SOC value of the

target according to the input and measurement information of the system in order to obtain an estimated SOC value. At the same time, an observation equation coefficient matrix c_k^j and residual r_k^j were generated. Then, according to c_k^j and r_k^j , the matching probability of the actual state of the battery with each circuit model was determined, thus providing an estimate of SOC and SOH.

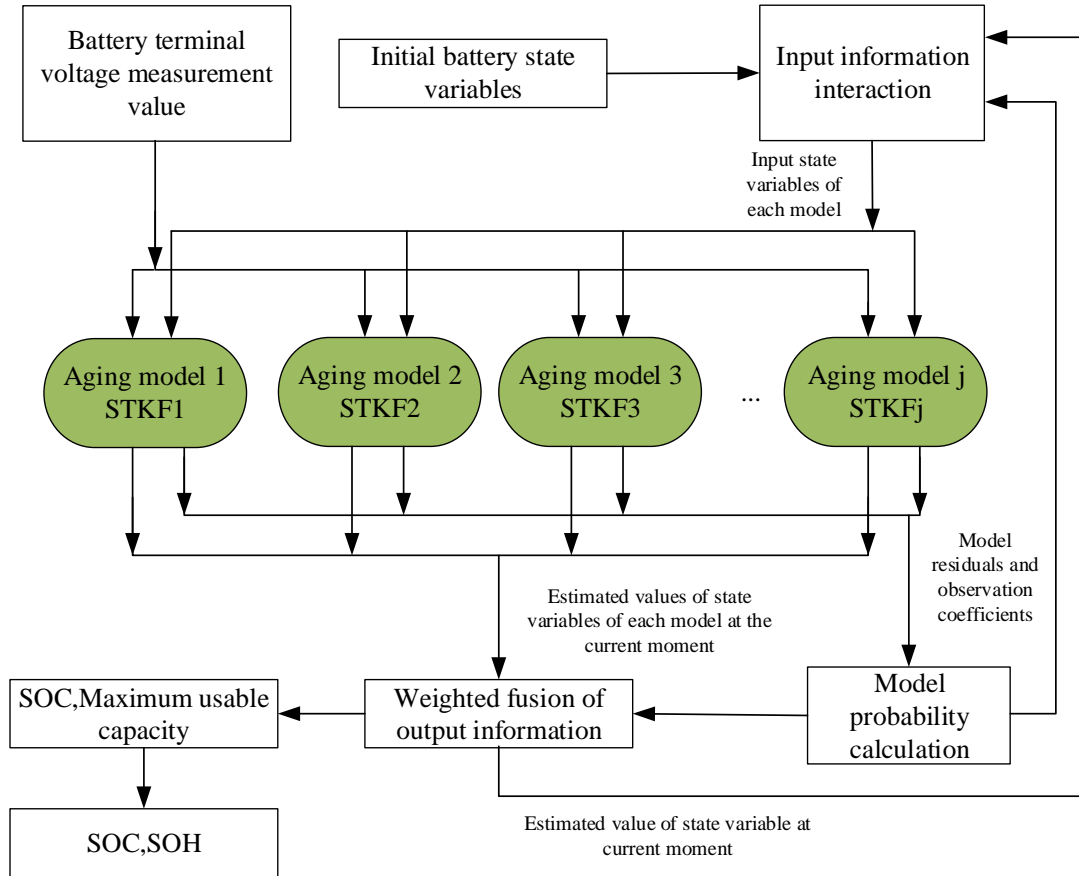


Figure 4. IMM algorithm flow chart.

The system state equation and measurement equation of the j -th aging model are:

$$\begin{cases} X_k^j = f_{k-1}^j(X_{k-1}^j, \Phi_{k-1}) + w_{k-1}^j \\ Z_k = h_k^j(X_k^j, \Phi_k) + v_k \end{cases} \quad (22)$$

Each model possessed a separate filter to represent its state. IMM controls the transformation and information exchange between various models through a Markov TPM. The TPM composed of the j aging model in the battery multi-model simulation system can be expressed as:

$$\Pi = \{\pi^{ij}\}_{l \times l} \quad (23)$$

$$\pi^{ij} = P\{m(k) = m_j | m(k-1) = m_i\}, \quad \forall i, j \in \{1, 2, \dots, l\} \quad (24)$$

$$\sum_{j=1}^m \pi^{ij} = 1, \quad 0 \leq \pi_{ij} \leq 1 \quad (25)$$

Among them, the main diagonal element of Π is the model probability, and the non-main diagonal element is the mixed probability.

The IMM algorithm is mainly divided into four parts: input interaction, parallel filtering, model probability calculation and fusion output [53].

3.1 Input interaction.

The ordinary Kalman Filter algorithm directly uses the filtering result of the previous moment as the input value of the current moment, but the IMM algorithm interacts the filtering results of the previous moment, and then uses the interactive result as the input value of the aging model at the current moment. The TPM guided the input information of each model to interact according to the rules in equations (26) and (27), and also determined the transformation between models.

State estimate update:

$$\hat{X}_{k-1|k-1}^{0j} = \sum_{i=1}^l \hat{X}_{k-1|k-1}^i \mu_{k-1|k-1}^{ij} \quad (26)$$

Covariance update:

$$P_{k-1|k-1}^{0j} = \sum_{i=1}^l \mu_{k-1|k-1}^{ij} \left[P_{k-1|k-1}^i + (\hat{X}_{k-1|k-1}^i - \hat{X}_{k-1|k-1}^{0j})(\hat{X}_{k-1|k-1}^i - \hat{X}_{k-1|k-1}^{0j})^T \right] \quad (27)$$

$P_{k-1|k-1}^{0j}$ is the updated covariance, $\hat{X}_{k-1|k-1}^{0j}$ is the updated state estimate, and $\mu_{k-1|k-1}^{ij}$ is the mixed probability of other models transferring to model STKF_i. The formula can be expressed as:

$$\begin{cases} \mu_{k-1|k-1}^{ij} = \pi^{ij} \mu_{k-1}^i / \bar{c}_j \\ \bar{c}_j = \sum_{i=1}^r \pi^{ij} \mu_{k-1}^i \end{cases} \quad (28)$$

where μ_{k-1}^i is the model probability of model STKF_i at time $k-1$. \bar{c}_j represents the predicted probability of the model STKF_j.

3.2 Parallel filtering

Each strong tracking Kalman filter(STKF) in the IMM worked in parallel and independently. Each STKF represented an aging model and estimated the state of the battery based on system measurements and input variables. When the battery aging situation is altered, its model parameters changes accordingly, which can be directly reflected in the battery terminal voltage. Therefore, achieving accurate estimation of battery SOC may accurately estimate the battery terminal voltage. Compared with EKF and UFK, STKF produces smaller approximation errors when dealing with nonlinear systems and introduces a time-varying fading factor in order to force the residuals to be orthogonal, thereby improving the robustness of the model. The ability to track slow changes and sudden changes has been demonstrated to be extremely strong [54,55]. Therefore, STKF can be quite suitable for use as a filtering algorithm in battery SOC estimation.

Taylor expansion was performed according to the functions $f_{k-1}^j(X_{k-1}^j, \Phi_{k-1})$ and $h_k^j(X_k^j, \Phi_k)$ in the STKF_j model given by equation (22), where the first and zeroth order terms were kept in order to

obtain:

$$\begin{cases} f_{k-1}^j(X_{k-1}^j, \Phi_{k-1}) \approx f_{k-1}^j(\hat{X}_{k-1}^j, \Phi_{k-1}) + \frac{\partial f_{k-1}^j(\hat{X}_{k-1}^j, \Phi_{k-1})}{\partial X_{k-1}^j} \Big|_{X_{k-1}^j = \hat{X}_{k-1}^j} (X_{k-1}^j - \hat{X}_{k-1}^j) \\ h_k^j(X_k^j, \Phi_k) \approx h_k^j(\hat{X}_k^j, \Phi_k) + \frac{\partial h_k^j(\hat{X}_k^j, \Phi_k)}{\partial X_k^j} \Big|_{X_k^j = \hat{X}_k^j} (X_k^j - \hat{X}_k^j) \end{cases} \quad (29)$$

Simplifying the above expression:

$$A_k^j = \frac{\partial f_k^j(\hat{X}_k^j, \Phi_k)}{\partial X_k^j} \Big|_{X_k^j = \hat{X}_k^j}, C_k^j = \frac{\partial h_k^j(\hat{X}_k^j, \Phi_k)}{\partial X_k^j} \Big|_{X_k^j = \hat{X}_k^j} \quad (30)$$

Then, equation (22) can be expressed as:

$$\begin{cases} X_k^j = A_k^j X_{k-1}^j + f_{k-1}^j(\hat{X}_{k-1}^j, \Phi_{k-1}) - A_k^j \hat{X}_{k-1}^j + w_{k-1}^j \\ Z_k = C_k^j X_k^j + h_k^j(\hat{X}_k^j, \Phi_k) - C_k^j \hat{X}_k^j + v_k \end{cases} \quad (31)$$

For the nonlinear system corresponding to equation (22), the designed strong tracking Kalman filter is:

$$\hat{X}_{k+1}^j = \hat{X}_k^j + L_k^j r_k^j \quad (32)$$

in:

$$r_k^j = Z_k - h_k^j(\hat{X}_k^j, \Phi_k) \quad (33)$$

In this paper, r_k^j referred to the terminal voltage residual of the battery under the j model, from which the model parameter information of the battery can be extracted to determine the state information of the battery. If the output of one of the aging models exactly matched the output of the actual system, a residual with a zero-mean value was generated. If incorrect, the battery system operated in this aging state so as to determine the estimated SOC. If the output of one of the aging models was unable to completely match the output of the actual system, a non-zero residual error was generated. The residual value r_k^j and observation matrix C_k^j can determine the matching probability of the model as well as the actual situation of the current battery, after which it can ascertain the estimated value of SOC. Following determination of the SOC value of each model, IMM adopted a method based on model probability in order to estimate SOC and battery capacity. The estimation of SOC and battery capacity is introduced in the following section.

STKF achieved strong tracking characteristics by determining the gain matrix L_k^j online, which required L_k^j to satisfy equation (34):

$$\begin{cases} E[(X_k^j - \hat{X}_k^j)][(X_k^j - \hat{X}_k^j)^T] = \min \\ E[r_k^j (r_k^j)^T] = 0 \end{cases} \quad (34)$$

Equation (34) indicated that when the difference between the actual value and the estimated state value was large, L_k^j needed to be determined online. This ensured that the residuals were orthogonal, and can achieve error-free tracking of the system. If the difference between the actual value and the state estimated value was small, then STKF degenerated to EKF. In this way, the amount of calculation of STKF was also more moderate.

Equation (35) was the error covariance matrix:

$$P_k^j = \lambda_k^j A_{k-1}^j P_{k-1}^j A_{k-1}^j + Q_{k-1}^j \quad (35)$$

λ_k^j was the fading factor, and $\lambda_k^j \geq 1$.

The fading factor was solved:

$$\lambda_k^j = \begin{cases} e_k^j, & e_k^j > 1 \\ 1, & e_k^j \leq 1 \end{cases} \quad (36)$$

Where $e_k^j = \text{tr}(N_k^j) / \text{tr}(M_k^j)$, N_k^j and M_k^j were defined as:

$$\begin{cases} N_k^j = E_{0,k}^j - \beta^j R_k - C_k^j Q_{k-1}^j (C_k^j)^T \\ M_k^j = C_k^j A_{k-1}^j P_{k-1}^j (A_{k-1}^j)^T (C_k^j)^T \end{cases} \quad (37)$$

In the above formula, the calculation formula of the residual covariance matrix $E_{0,k}^j$ was:

$$E_{0,k}^j = \begin{cases} r_1^j (r_1^j)^T & (k=1) \\ \frac{\delta E_{0,k-1}^j + r_k^j (r_k^j)^T}{1+\delta} & (k>1) \end{cases} \quad (38)$$

δ was the forgetting factor, β was the weakening factor, and $\beta \geq 1$.

Thus, the Kalman gain matrix was:

$$L_k^j = P_k^j (C_k^j)^T [C_k^j P_k^j (C_k^j)^T + R_k]^{-1} \quad (39)$$

The error covariance update matrix was:

$$P_k^j = (I - L_k^j C_k^j) P_{k-1}^j \quad (40)$$

where I was the identity matrix.

3.3 Model probability calculation

The estimation of SOC and SOH was determined by the model probability μ_k^j . The model probability μ_k^j was updated according to the likelihood function method, in which the likelihood function of the model *STKFj* is:

$$\Lambda_k^j = \frac{e^{-\frac{1}{2}(r_k^j)^T r_k^j (S_k^j)^{-1}}}{2\pi^{n/2} |S_k^j|^{1/2}} \quad (41)$$

in:

$$\begin{cases} S_k^j = C_k^j P_{k|k-1}^j (C_k^j)^T + Q_k^j \\ r_k^j = Z_k - h_k^j(\hat{X}_k^j, \Phi_k) \end{cases} \quad (42)$$

Then, the model probability of the updated model *STKFj* is:

$$\mu_k^j = \frac{\Lambda_k^j \bar{c}_j}{\sum_{j=1}^r \Lambda_k^j \bar{c}_j} \quad (43)$$

The value of the probability μ_k^j of each model represented its matching degree with the current calculation model. The probability of each model interacted with the estimated value of the model in order to obtain the final estimate of SOC and battery capacity.

Combining equation (28) and equation (43), model probability μ_k^j was shown to determine the

estimation result of SOC and battery capacity, while mixing probability $\mu_{k-1|k-1}^{ij}$ determined the mixing of input information, thereby affecting residual r_k^j . Meanwhile, μ_k^j and $\mu_{k-1|k-1}^{ij}$ were determined by TPM. Since the TPM only carries a small amount of model history information in order to carry out rapid model response conversion. This can result in the reduction of delays in SOC and SOH estimation.

3.4 Fusion output

Weighted merging of the model probabilities with the estimates for each filter to obtain:

The estimated state of the system is:

$$\hat{X}_{k|k} = \sum_{i=1}^j \hat{X}_{k|k}^i \mu_k^i \quad (44)$$

The state estimate variance of the fusion is:

$$P_{k|k} = \sum_{i=1}^j \mu_k^i [P_{k|k}^i + (\hat{X}_{k|k}^i - \hat{X}_{k|k})(\hat{X}_{k|k}^i - \hat{X}_{k|k})^T] \quad (45)$$

The battery capacity after fusion is:

$$Q_{\text{NOW}} = \sum_{i=1}^j Q_i \mu_k^i \quad (46)$$

That is, the battery SOH after fusion is:

$$\text{SOH} = \frac{Q_{\text{NOW}}}{Q_{\text{NEW}}} \times 100\% \quad (47)$$

Q_{NOW} is the maximum usable capacity of the new battery.

The IMM algorithm cycle illustrates that the SOC estimation algorithm for the full life cycle of lithium-ion battery based on interactive multi-model was based on the current situation of the battery as well as the matching of each circuit in the battery multi-model simulation system, resulting in the final estimation of the state of the battery. Since the algorithm considered the historical information of the model at the current filtering time, it also mixed previous estimation information at the beginning of each cycle, avoiding defects pertaining to the complexity of the optimal estimation method that exponentially increased with time, which was deemed to be a positive change. This serves as a main difference in regard to interactive multi-model estimation compared to that of other estimation methods [56].

The proposed algorithm can be summarized according to the following. All models were first initialized, for which the initialization parameters included TPM π^{ij} , the probability matrix μ_k^i and covariance matrix P_k^j of the model, the coefficient A, B, C of the nonlinear equation and the parameters of the battery multi-model simulation system. Then, the inputted initial values of the state variables were used to obtain the weighted and fused SOC and SOH estimations through the IMM algorithm. Finally, the information at the current moment was fed back to the input terminal for state estimation at the next moment.

4. EXPERIMENTAL RESEARCH

The experimental object was Cylindrical Lithium-ion Cell model LR18650EH. Table I below shows the specific parameters of the battery. The experimental equipment was a battery cycle charger with the model LBT5V30A produced by Arbin. It can work normally in the range of -30A~30A and -5V~5V, the battery cycle charger and the experimental battery are shown in Fig. 5.



Figure 5. The battery cycle charger and battery.

Table I. Specific parameters of LR18650EH cell

No.	Item	Specificaiton
1	Weight	40±2.0g
2	Rated Capacity	1600mAh
3	Rated Voltage	3.2V
4	Voltage limit	2.0V~3.65V
5	Maximum Charge Current	1.0 C
6	Operating Temperature	-20°C~ 60°C

In order to verify the effectiveness of the proposed method for estimating the SOC for the entire life cycle of lithium-ion batteries, LR18650EH batteries with different degrees of aging were selected as the research object, regardless of the impact of temperature on the battery. In doing so, by using 1C current to charge and discharge the battery in cycles, batteries with different aging states can be obtained.

Considering that the battery model parameters change slowly during the charging and discharging experiments, the parameters were identified once every 50 cycles for a total of 50 times. The parameter identification method was previously outlined in section 2.2. Different model parameters represent different aging states of the battery. Therefore, models of different aging states in the full life cycle of the battery can be obtained. Considering the complexity of the Algorithm and the estimation precision of SOC, the experiment took 4 aging models, which are SOH = 100% circuit model, SOH = 70% circuit model, SOH = 40% circuit model, SOH = 10% circuit model, I. E. $j = 4$ in Fig. 4.

This study conducted two sets of experiments to verify the effectiveness of the IMM-STKF

algorithm: (a) experiments under HPPC conditions; and (b) experiments under DST conditions. In these experiments, the STKE algorithm proposed in the literature [29] was introduced for comparison, after which the SOC estimation effect of the two algorithms was observed.

4.1. Verifying the experimental results under HPPC working conditions

In this study, a battery with a rated capacity of 1600mAh was attenuated to 1450mAh for 6200s using Hybrid Pulse Power Characteristic (HPPC) experiments to verify the effectiveness of the algorithm.

The current and voltage data obtained by the lithium-ion battery HPPC experiment are shown in Fig. 6. The battery was discharged with a current of 1C for 60 seconds, which was then rested for 61 seconds. A total of 50 cycles were performed. The parameters identified in this process were used as the model parameters. Fig. 7 depicts the voltage error curve, in which the identified voltage root mean square error (Root mean square error, RMSE) was found to be 2.45 mV, and the mean absolute error (MAE) was 2.1813 mV. The FFRLS algorithm was shown to have a very high parameter identification accuracy. Fig. 8 illustrates the SOC estimation results based on IMM-STKF and ordinary STKF, while Fig. 9 shows the SOC estimation error curve. The RMSE of STKF and IMM-STKF were observed to be 1.05% and 0.25%, respectively, while the MAE of STKF and IMM-STKF were 0.82% and 0.20%, respectively. Table II show that the IMM-STKF algorithm proposed in this paper had higher estimation accuracy than the STKF algorithm proposed in the literature [29]. Fig. 10 represents the capacity estimation curve, where the initial error was shown to be 150mAh. When the charge and discharge current was 0, the capacity was unable to be corrected. With the associated iteration, the maximum usable capacity was better estimated. The corresponding SOH value was obtained through the definition of SOH, as shown in Fig. 11. As shown in Figs. 8, 9 and 11, when the battery just began to discharge, the estimation accuracy of SOC and SOH were found to be low, and the estimation accuracy of them rose over time. Therefore, the estimation algorithm based on IMM-STKF was able to perform SOC estimation in the battery life cycle.

$$RMSE = \sqrt{\frac{\sum_{i=1}^n (p_i - a_i)^2}{n}} \quad (48)$$

$$MSE = \frac{\sum_{i=1}^n |a_i - p_i|}{n} \quad (49)$$

In the above formula: a=actual target; p=predicted target.

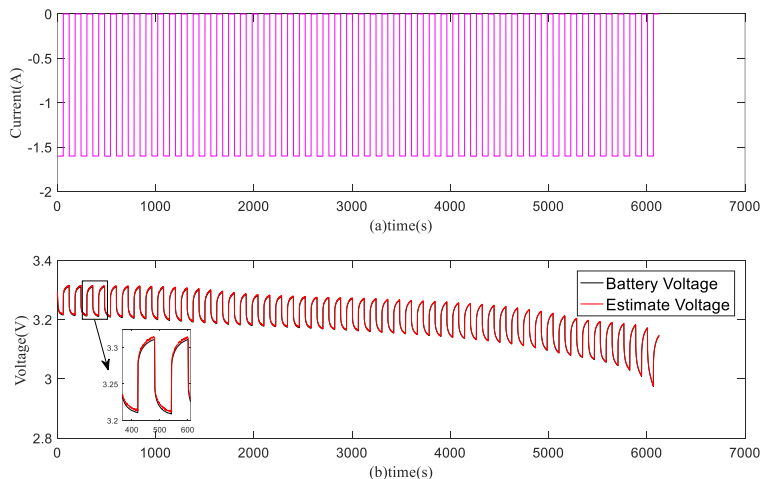


Figure 6. HPPC experiment: (a) current curve; (b) voltage curve.

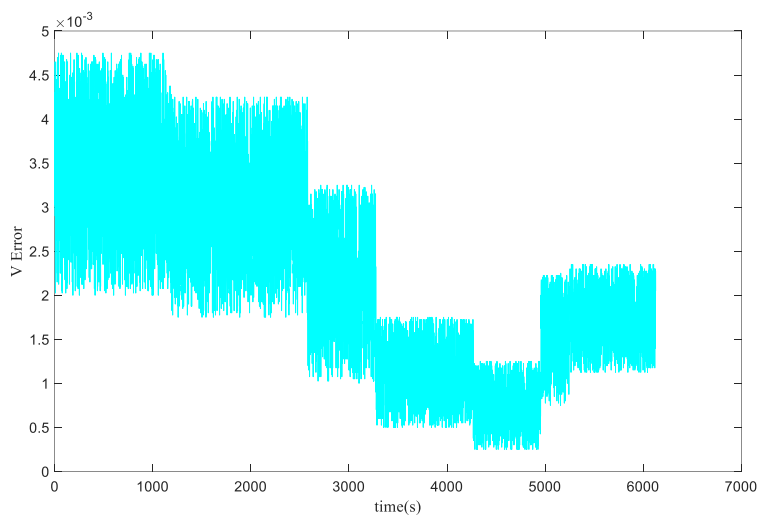


Figure 7. The voltage error curve of the HPPC experiment.

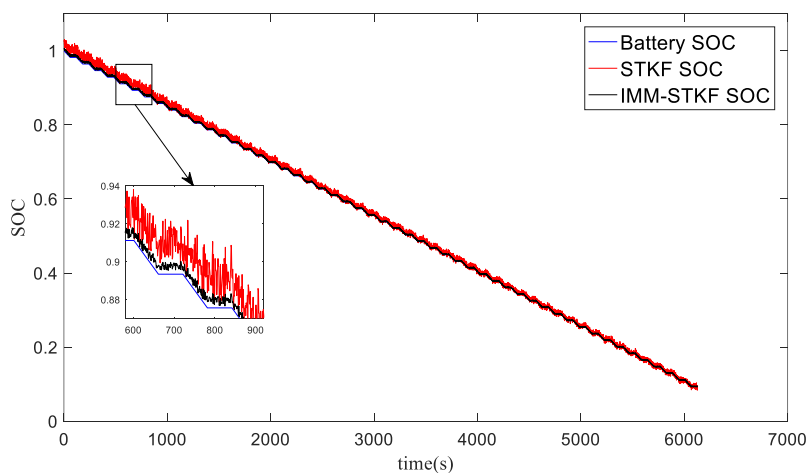


Figure 8. SOC estimation result of HPPC experiment.

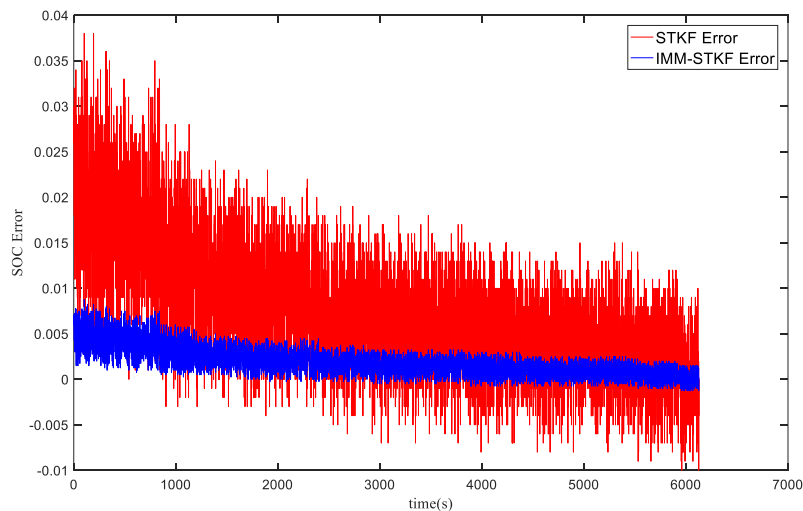


Figure 9. SOC estimation error of HPPC experiment.

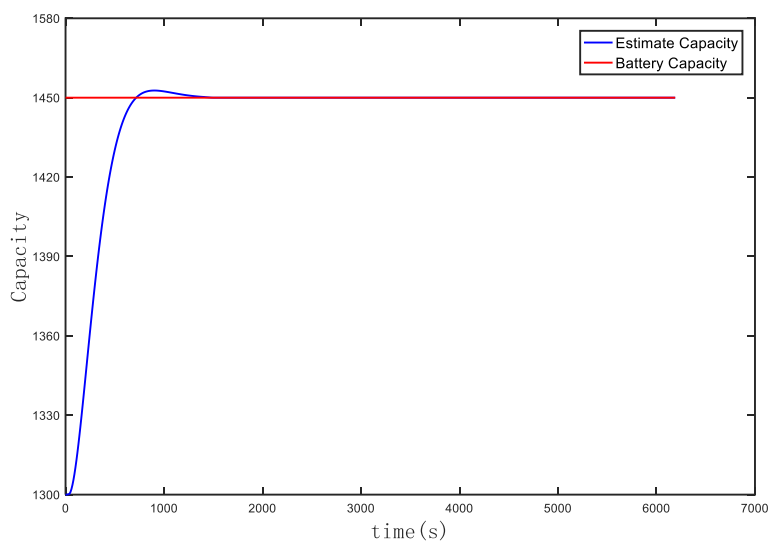


Figure 10. Estimation of the maximum usable capacity of the HPPC experiment.

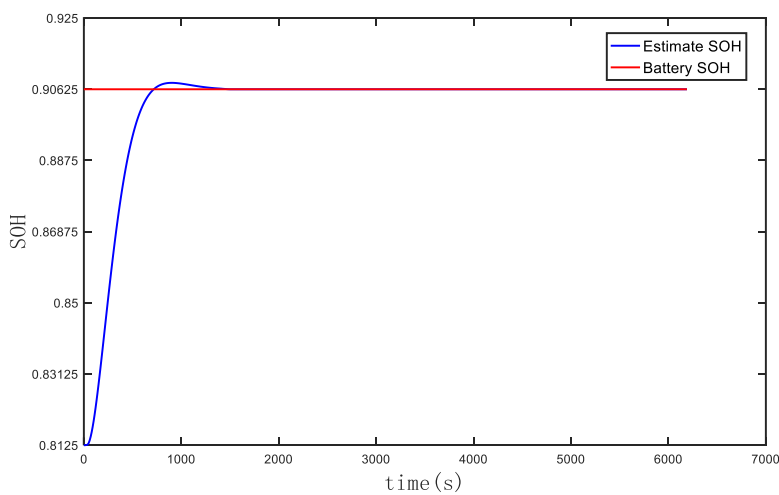


Figure 11. SOH estimation result of HPPC experiment.

4.2. Verifying experimental results under DST conditions

In order to further verify the effectiveness of the algorithm, a 16000s dynamic stress test (DST) experiment was performed on a battery with a rated capacity of 1600mAh attenuated to 1400mAh.

The current and voltage data obtained by the DST experiment of lithium-ion batteries are shown in Fig. 12, for which the parameters identified in this process were used as the model parameters. The voltage error curve is shown in Fig. 13, where the RMSE of the actual voltage and the identification voltage was 3.02mV, while the MAE was 2.61mV. The FFRLS algorithm was demonstrated to have a high parameter identification accuracy for the DST operating condition experiments of the battery. The SOC estimation results based on IMM-STKF and ordinary STKF are shown in Fig. 14, for which the SOC estimation error is shown in Fig. 15. The RMSE of STKF and IMM-STKF were noted to be 1.11% and 0.23%, respectively, while the MAE of STKF and IMM-STKF were 0.96% and 0.19%, respectively. Table II show that the IMM-STKF algorithm proposed in this paper had higher estimation accuracy than the STKF algorithm proposed in the literature [29]. Fig. 16 depicts the capacity estimation curve, where initial error was recorded to be 200mAh. When the charge and discharge current was 0, the capacity was unable to be corrected. With the battery was charged and discharged, the maximum usable capacity was estimated. The corresponding SOH value was obtained through the definition of SOH, as shown in Fig. 17. Figs. 13, 14 and 17, show that when the battery just began to discharge, the estimation accuracy of SOC and SOH were low, and the estimation accuracy of them rose over time. Therefore, the estimation algorithm based on IMM-STKF can carry out SOC estimation in the battery life cycle.

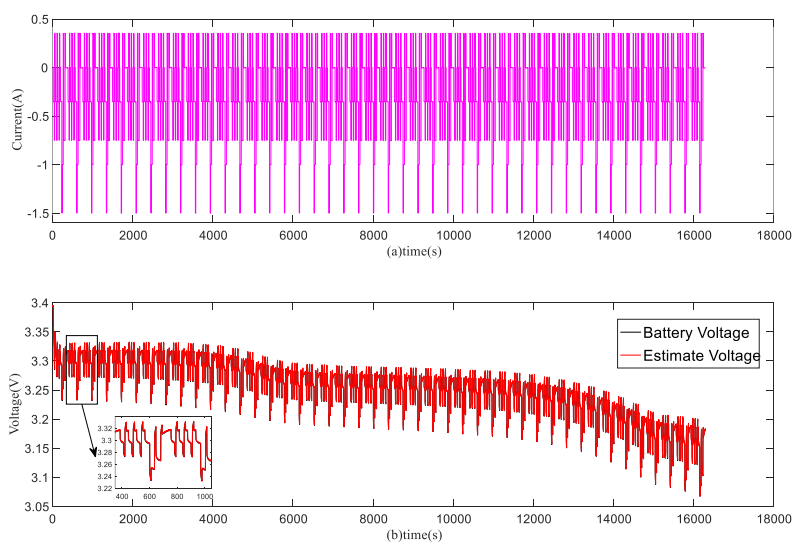


Figure 12. DST experiment: (a) current curve; (b) voltage curve.

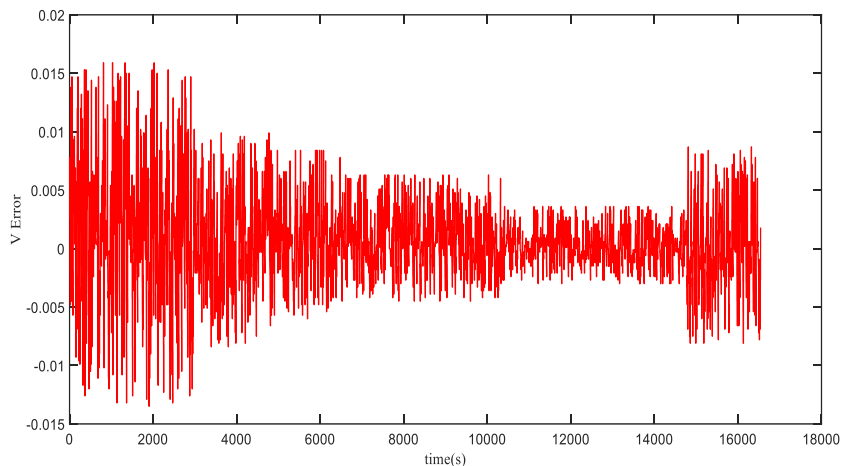


Figure 13. Voltage error curve of DST experiment.

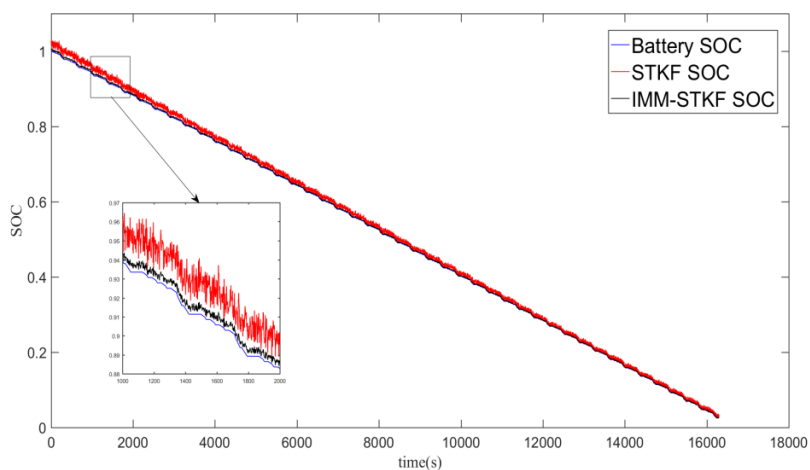


Figure 14. SOC estimation result of DST experiment.

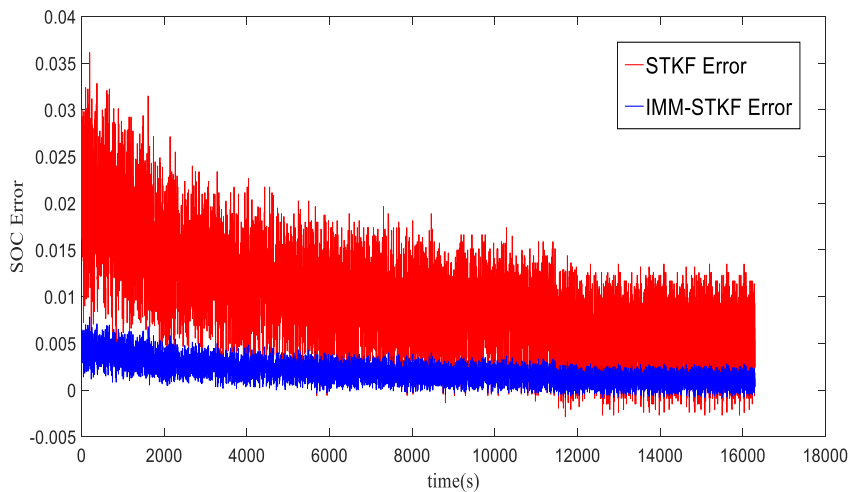


Figure 15. SOC estimation error of DST experiment.

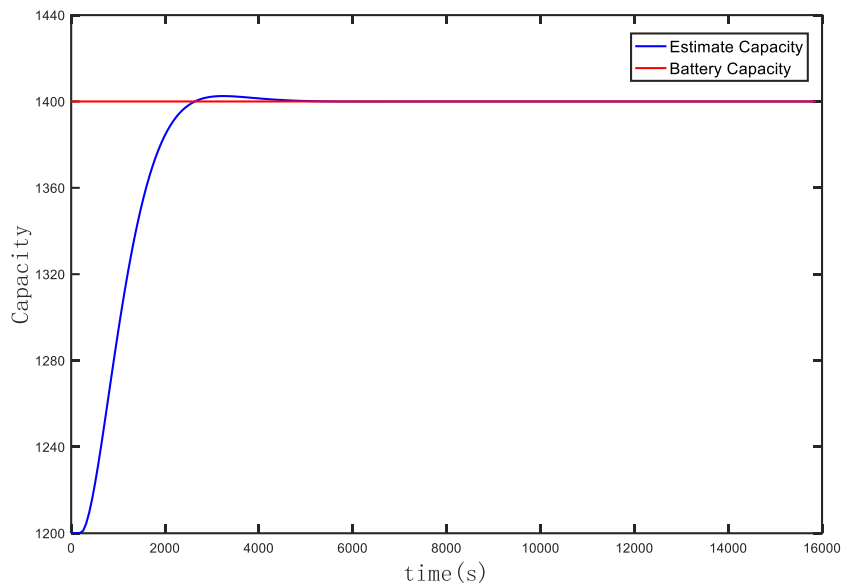


Figure 16. Estimation of the maximum usable capacity of the DST experiment.

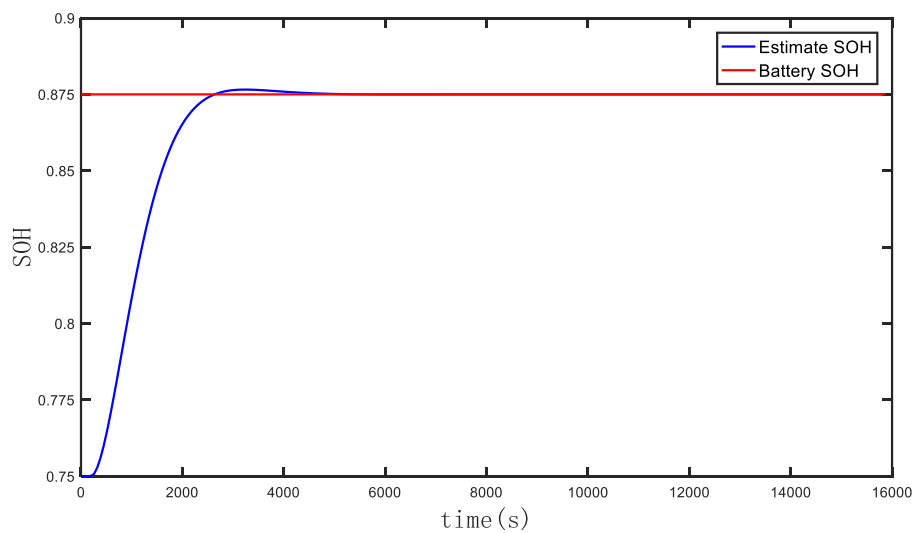


Figure 17. SOH estimation result of DST experiment.

Table II. Errors of SOC estimation results

MAE	Algorithm	HPPC		DST	
		RMSE		MAE	RMSE
	STKF(%)	0.82	1.05	0.96	1.11
	IMM-STKF(%)	0.20	0.25	0.19	0.23

5. CONCLUSION

In order to address difficulties in accurately estimating the SOC during the entire life cycle of lithium-ion batteries, this paper proposed an interactive multi-model-based SOC estimation algorithm for lithium-ion batteries, and the accurate estimation of SOC in the whole life cycle of the battery was realized by combining with STKF. The proposed algorithm introduced an IMM-compliant TPM in order to enable the real-time interaction of input information for each aging model. In addition, the output terminal inputted the updated probability information of each aging model to the input terminal of the filter according to the TPM, thus improving the accuracy of SOC estimation. In terms of the STKF and IMM-STKF algorithms, both were shown to be able to estimate SOC, however, their estimation accuracy differed. Specifically, the IMM-STKF algorithm was shown to possess a higher estimation accuracy. During the HPPC experiment, according to the STKF algorithm, the MAE of the SOC was estimated to be 0.82%, while the RMSE was 1.05%. Moreover, based on the IMM-STKF algorithm, the MAE of the SOC was estimated to be 0.20%, while the RMSE was 0.25%. In the DST experiment, in light of the STKF algorithm, the SOC MAE was estimated to be 0.96%, while the RMSE was 1.11%. Finally, in terms of the IMM-STKF algorithm, the SOC MAE was estimated to be 0.19%, while the RMSE was 0.23%. The corresponding findings of this study clearly shows that the IMM-STKF algorithm can better estimate the SOC of the battery under different working conditions. In addition, the IMM-STKF algorithm can estimate the SOH of the battery while estimating the SOC, thus attaining SOC estimation of the whole life cycle of the lithium-ion battery. Therefore, the IMM-STKF algorithm can accurately estimate the SOC during the full life cycle of the battery.

CONFLICTS OF INTEREST

The authors declare that they have no known financial nor personal interest that could have had an influence in the work reported in this paper.

ACKNOWLEDGMENTS

This work was supported by the joint fund project of the Ministry of Education of China (multi-transmitter/single-receiver coil underwater wireless charging system); Advance Research Project of Equipment of China(41421040301).

References

1. J.P. Wen, D. Zhao, C.W. Zhang, *Renewable Energy*, 162(2020)1629-1648.
2. Y. Zhang, X.Y. Yuan, L. Duan, L. Jiang, *Journal of Energy Engineering*, 147 (2021) 04021049.
3. D. How, M A. Hannan, M. Lipu, *IEEE Access*, 7(2019)136116-136136.
4. X. Y. Li, T. Long, J. D. Tian, Y. Tian. *Journal of Power Sources*, 479(2020)228677.
5. X. Zhu, S. Gao, S. Yang, *Journal of Renewable & Sustainable Energy*, 8(2016) 376-378.
6. Y. Deng, Y. Hu, Y. Cao, An improved algorithm of soc testing based on open-circuit voltage-ampere hour method, *Intelligent Computing in Smart Grid and Electrical Vehicles(ICSEE)*, Springer, Berlin, Heidelberg, 2014, 258-267.
7. J. Sun, Y. Tang, J. Ye, T. Jiang , *Energy*, 243(2022)122882.
8. S. N. Kong, C. S. Moo, Y. P. Chen, Y.C. Hsieh. *Applied Energy*, 86 (2009)1506-1511.
9. J. Li, M. Liu, State-of-charge Estimation of Batteries Based on Open-circuit Voltage and Time

- Series Neural Network, *2019 6th International Conference on Systems and Informatics (ICSAI), Shanghai, China, 2019, 257-262.*
10. L. Ma, C. Hu, F. Cheng. *The Journal of Energy Storage*, 37(2021)102440.
 11. T. Smith, J. Garcia, G. Washington, *Journal of Energy Engineering*. 147.5 (2021)04021035.
 12. N. Guo, Y. Fang, Z. Tian, S. Cao, *The Journal of Engineering*, 15(2019)576-580.
 13. Q. Liu, Y. J. Shen, Research on soc estimation of battery based on bp neural network, *The 2020 International Conference on Internet of Things, Artificial Intelligence and Mechanical Automation (IoTAIMA), Hangzhou, China, 2020,012067*
 14. L. Zhang, K. Li, D. Du, Y. Guo, Z. Yang, *IEEE Access*, 8 (2020)156165-156176.
 15. C. Venkatesan, C. K. Patil, A. Karthick, G. Dharmaraj, A. Ghosh. *World Electric Vehicle Journal*, 12.1 (2021) 38.
 16. J. Sun, W. Liu, C. Tang, *IEEE Transactions on Power Electronics*, 36.7 (2021)7853-7865.
 17. J. Marcicki, M. Canova, A. T. Conlisk, G. Rizzoni, *Journal of Power Sources*, 237(2013) 310-324.
 18. L. Sharma, S. Bharathraj, P. Barpanda, S. P. Adiga, K. S. Mayya. *ACS Applied Energy Materials*, 4.1(2021)1021-1032.
 19. A. Rahmoun, H. Biechl, A. Rosin, *Electrical Control & Communication Engineering*, 2.1(2013)34-39.
 20. Z. Xia, J. A. Abu Qahouq, Evaluation of Parameter Variations of Equivalent Circuit Model of Lithium-ion Battery under Different SOH Conditions, *2020 IEEE Energy Conversion Congress and Exposition (ECCE), Detroit, MI, USA, 2020, 1519-1523.*
 21. L. Chen, Z. Lü, W. Lin, J. Li, H. Pan, *Measurement*, 116(2018)586-595.
 22. R. Xiong, Y. Zhang, H. He, Z. Xuan, M. G. Pecht, *IEEE Transactions on Industrial Electronics*, 65.2 (2017)1526-1538.
 23. Z. Xia, J. Qahouq, Adaptive and Fast State of Health Estimation Method for Lithium-ion Batteries Using Online Complex Impedance and Artificial Neural Network, *2019 IEEE Applied Power Electronics Conference and Exposition (APEC), Anaheim, CA, USA, 2019,3361-3365.*
 24. L. Fang, J. Lin, P. Bo, *Energy Procedia*, 158(2019)3008-3013.
 25. U. Westerhoff, T. Kroker, K. Kurbach, M. Kurrat, *The Journal of Energy Storage*, 8(2016)255-256.
 26. L. Guo, J. Li, Z. Fu. *Energy Procedia*, 158(2019)2599-2604.
 27. Z. Huang, Y. Fang, J. Xu, *International Journal of Automotive Technology*, 22.2(2021)335-340.
 28. J. Wang, Z. Zhang, Lithium-ion Battery SOC Estimation Based on Weighted Adaptive Recursive Extended Kalman Filter Joint Algorithm, *2020 IEEE 8th International Conference on Computer Science and Network Technology (ICCSNT), Dalian, China, 2020,11-15.*
 29. Y. Zhao, *Journal of Shen-yang University of Technology*, 40(2018)192-197.
 30. J. H. Lee, I. S. Lee, *Energies*, 14.15(2021)4506.
 31. T. Kim, Q. Wei, L. Qu, Online SOC and SOH estimation for multicell lithium-ion batteries based on an adaptive hybrid battery model and sliding-mode observer, *2013 IEEE Energy Conversion Congress and Exposition, Denver, CO, USA, 2013, 292-298.*
 32. J. Li, M. Ye, K. Gao, X. Xu, S. Jiao, *International Journal of Energy Research*, 45(2021) 13307-13322.
 33. X. Xia, M. Liu, *Information and Control*, 5 (2017)13-18.
 34. X. Xia, S. Li, Z. Meng, *CACRE2019*, 2 (2019)1-6.
 35. H. Blom, An efficient filter for abruptly changing systems, *The 23rd IEEE Conference on Decision and Control, Las Vegas, NV, USA, 1984, 656-658.*
 36. Y. Wang, D. Meng, R. Li, Y. Zhou, X. Zhang, *International Journal of Energy Research*, 45 (2021) 13198-13218.
 37. B. Meng, Y. Wang, J. Mao, J. Liu, G. Xu, J. Dai. *Energies*, 11(2018)586.
 38. A. Fotouhi, D. J. Auger, K. Propp, S. Longo, M. Wild, *Renewable and Sustainable Energy Reviews*, 56(2016)1008-1021.
 39. K. S. Hariharan, V. S. Kumar, *Journal of power sources*, 222 (2013)210-217.

40. X. Hu, S. Li, H. Peng, *Journal of Power Sources*, 198(2012)359-367.
41. P. Shrivastava, T. K. Soon, M. Idris, S. Mekhilef, *Renewable and Sustainable Energy Reviews*, 113(2019) 109233.
42. J. Newman, K. E. Thomas, H. Hafezi, D. R. Wheeler, *Journal of Power Sources*, 119(2003) 838-843.
43. X. Hu, S. Li, H. Peng, F. Sun, *Journal of Power Sources*, 217(2012)209–219.
44. A. Ing, R. Masoudi, J. McPhee, T. S. Dao, Comparison of Optimization Techniques for Lithium-Ion Battery Model Parameter Estimation, *SAE 2014 World Congress & Exhibition, Detroit, Michigan, USA, 2014*,01-1851.
45. Y. Wang, C. Zhang, Z. Chen, *Applied Energy*, 137 (2015)427-434.
46. J. Feng, Y. L. He, R. Bao, *Advanced Materials Research*, 490(2012)3854-3858.
47. R. Li, Z. Wang, J. Yu, Y. Lei, Y. Zhang, J. He, Dynamic Parameter Identification of Mathematical Model of Lithium-Ion Battery Based on Least Square Method, *2018 IEEE International Power Electronics and Application Conference and Exposition (PEAC), Shenzhen, China, 2018*, 1-5.
48. R. Zhu, B. Duan, F. Wen, J. Zhang, C. Zhang, *Journal of Mechanical Engineering*, 55(2019)85-93.
49. J. Feng, W. Long, K. Huang, J. Lu, X. Zhang, *Energy Storage Science and Technology*, 10(2021) 242.
50. G. Xie, L. Sun, T. Wen, X. Hei, F. Qian, *IEEE Transactions on Systems, Man, and Cybernetics: Systems*, 51.5(2019)2980-2989.
51. P. K. Jawahar, V. Vaidehi, D. E. Nirmala, *Wireless Personal Communications*, 65(2012) 67-81.
52. J. Yun, C. K. Ryoo, *Journal of Guidance Control and Dynamics*, 37(2014)484-496.
53. Y. Wang, D. Meng, R. Li, Y. Zhou, X. Zhang, *IEEE Access*, 9(2021)18465-18480.
54. D. J. Jwo, C. M. Huang, An Adaptive Fuzzy Strong Tracking Kalman Filter for GPS/INS Navigation, *IECON 2007 - 33rd Annual Conference of the IEEE Industrial Electronics Society, Taipei, Taiwan, 2007*, 2266-2271.
55. X. Chen, C. Shen, W. B. Zhang, M. Tomizuka, Y. Xu, K. Chiu, *Measurement*, 46(2013)3847-3854.
56. C. Hoffmann, T. Dang, *Robotics and Autonomous Systems*, 57(2009)268-278.